

Optimal Sizing and Energy Management of Hybrid Energy Storage Systems for Electric Vehicles

Huilong Yu, Francesco Castelli-Dezza and Federico Cheli

Abstract—Hybrid energy storage system (HESS) with the combination of lithium-ion batteries and supercapacitors has been recognized as a quite appeal solution to face against the drawbacks such as, high cost, low power density and short cycle life of the battery-only energy storage system, which is the major headache hindering the further penetration of electric vehicles. A properly sized HESS and an implementable real-time energy management system are of great importance to achieve satisfactory driving mileage and battery cycle life, however, the introduced sizing and energy management problems are quite complicated and challenging in practice. This work proposed a Bi-level multi-objective sizing and control framework with the non-dominated sorting genetic algorithm-II and fuzzy logic control (FLC) as key components to obtain an optimal sized HESS and a corresponding optimal real-time FLC based EMS simultaneously. In particular, a vectorized fuzzy inference system which allows large scale fuzzy logic controllers operating in parallel is devised for the first time for such kinds of problems to improve the optimization efficiency. At last, the Pareto optimal solutions of different HESSs incorporating both optimal design and control parameters are obtained and compared to show the achieved enhancements.

Index Terms—Hybrid energy storage system; Lithium-ion Battery; Supercapacitor; vectorized fuzzy interface; multi-objective energy management; electric vehicles.

I. INTRODUCTION

In recent years, the challenges of air pollution, fossil oil crisis, and greenhouse gas emissions have aroused unprecedented amount of attentions on Electric vehicles (EVs) from the governments, academia and industries all over the world. After intensively developing over the last decades, the worldwide promotion and application of EVs have reached a considerable scale. However, the dynamic performance, cost, durability of an EV are still closely related to the design, integration, and control of its energy storage system (ESS) [1]. It is generally known that the battery-only ESS with high cost and short cycle life has become one of the biggest obstacles hindering further penetrations of the EVs. Lithium-ion battery-only ESS with high energy density and relatively good power density dominate the most recent group of EVs in development, however, its degradation can be accelerated when there is high peak discharging/charging power demand during the operation process [2]–[4]. Alternatively, supercapacitors (SCs) can tolerate much more charging/discharging cycles

and exhibit superior ability to cope with high peak power, due to their specific energy storage mechanism, but the low energy density hampers their large scale application on EVs [5], [6]. A hybrid energy storage system (HESS) introduced also SCs which can bridge the gap between them is considered as one of the most promising solutions to solve the forgoing problems entrenched in battery-only/SC-only energy [7]–[9]. The configuration of a HESS vary with different connections of the battery, supercapacitor and DC/DC converter. The employed HESS in this work is the most studied configuration that using a bidirectional DC/DC converter to connect the supercapacitor with the battery in parallel, in which case, the voltage of supercapacitor can be adjusted in a wider range [8]. Existing research has demonstrated that HESS can dramatically improve braking energy recuperation efficiency, eliminate the need for battery over-sizing, and reduce the weight and cost of the entire system [10]. However, the application of HESS has introduced complicated sizing and energy management problems [11].

Finding the specific number of supercapacitor banks and battery cells that can minimize the cost, mass, energy consumption and battery degradation of the HESS is the so called HESS sizing problem. A sample-based global Dividing RECTangles (DIRECT) optimization algorithm is implemented to solve a formulated multi-objective sizing problem of the HESS [12]. While the non-dominated sorting genetic algorithm II (NSGA-II) is applied to obtain the Pareto frontier of battery degradation and total cost in designing a semi-active HESS [13]. [1], [14] proposed to solve the sizing problems of different HESSs with convex optimization algorithm.

The energy management strategy (EMS) of HESS aims to allocate the energy request between different energy sources for achieving desired performances, both the rule based and optimization based approaches are comprehensively investigated in previous work [15]. A time efficient utility function-based control of a semi-active HESS was proposed and carried out in [16] by formulating a weighted multi-objective optimization problem, then the formulated problem is solved based on the Karush-Kuhn-Tucker (KKT) conditions. Ref. [17] proposed an energy management strategy for a HESS based on fuzzy logic supervisory wavelet-transform frequency decoupling approach, which aims to maintain the state of the energy (SOE) of the supercapacitor at an optimal value, to increase the power density of the ESS and to prolong the battery lifetime. An explicit model predictive control system for a HESS was proposed and implemented in [18] to make the HESS operating within specific constraints while distributing current changes with different ranges and frequencies respectively

H. Yu was with the Department of Mechanical Engineering, Politecnico di Milano, 20156, Milano, Italy. He is now with University of Waterloo, N2L 3G1, Waterloo, Canada (e-mail: huilong.yu@uwaterloo.ca).

F. Cheli and F. Castelli Dezza are with the Department of Mechanical Engineering, Politecnico di Milano, 20156, Milano, Italy (e-mail: federico.cheli@polimi.it; francesco.castellidezza@polimi.it).

between the supercapacitor and battery. Ref. [19] developed a real-time predictive power management control strategy based on neural network and particle swarm optimization algorithm to minimize the integral cost including battery degradation and energy consumption. A variable charging/discharging threshold method and an adaptive intelligence technique based on historical data was proposed in [20] to improve the power management efficiency and smooth the load of a HESS. Two real-time energy management strategies based on KKT conditions and neural network were investigated and validated with experimental work in [21] to improve the battery state of health performance of a HESS effectively.

The continuous previous efforts have improved the overall performances of HESS considerably. However, most of the aforementioned work researched only on either the sizing or the energy management problem, in which case, the global optimal performance can not be achieved since the design and control problems of HESS are mostly coupled in fact [22]. Only sub-optimal solution is available when try to optimize the sizing and control parameters separately due to the reduced searching space. Some of the existing approaches in literature [1], [23] are off-line which are quite useful as the reference in designing real-time EMS but not appropriate for real implementation. Besides, most of the real-time implementable EMSs are mostly manually devised in the existing efforts which are not able to achieve the optimal performances.

Considering the drawbacks of the state-of-the-art methods, this work will investigate the HESS sizing and real-time control problem as a coupled problem. In particular, the HESS of an electric race car is investigated as a case study. Although win the race is the only ultimate goal on a circuit, we should try to minimize the cost for a racing team and the environmental impact caused by the waste battery as much as possible during a race or for the offline training, which can match the spirit of the electric racing better. Our goal of this work is to introduce the HESS with proper sizing parameters and optimized real-time EMS to improve the cycle life of the battery without scarifying the mileage of the electric race car too much. A multi-objective optimal sizing and control framework incorporating the battery model, supercapacitor model, evaluation model and a devised vectorized fuzzy inference system is proposed in this work. With this framework, the Pareto optimal solutions of the formulated multi-objective optimal sizing and control problem can be obtained, besides, both the optimal sizing and the static parameters of a fuzzy logic control (FLC) based EMS can be achieved simultaneously for all the solutions on the Pareto frontier which then can be implemented for real-time application.

The remainder of this work is divided into six parts. Section 2 elaborates the proposed Bi-level optimal design and energy management framework, then presents the formulation of the sizing and energy management problem. Section 3 describes the employed the battery and supercapacitor models. Section 4 gives the details of the devised FLC based on vectorized fuzzy inference engine. In section 5, the simulation parameters and settings are presented in detail. Section 6 demonstrates the obtained results and Section 7 illustrates the conclusions.

II. BI-LEVEL OPTIMAL DESIGN AND CONTROL FRAMEWORK

The proposed Bi-level optimal design and control framework is presented as Figure 1. The power demand of the driving profile P_{dem} , the battery state of charge x_{SOC} and supercapacitor state of energy x_{SOE} are the inputs of the FLC based EMS, while the outputs are requested power from the battery P_{reqbat} and from the supercapacitor P_{reqsc} . The outputs of the EMS are the inputs of the battery and supercapacitor modeled in Section III, while the evaluation indexes can be calculated with the outputs of the battery and supercapacitor model.

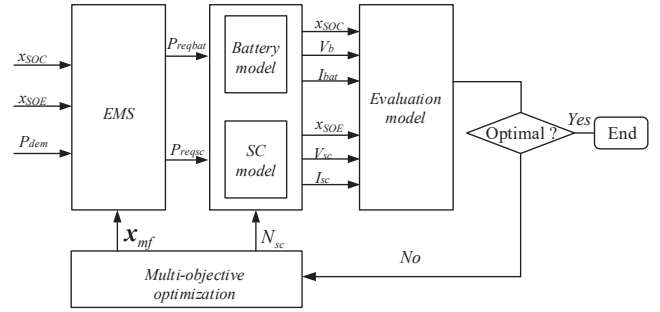


Fig. 1. Framework of the Bi-Level optimal design and control

The working scheme of the Bi-level optimal design and control is illustrated as follows. Firstly, the multi-objective algorithm will generate the sizing parameter matrix and the corresponding static tuning parameter matrix of the energy management system, in this work, the mentioned matrices are respectively the number of supercapacitor banks and the parameters of the membership functions (MFs) in different pages of the optimization parameters. Secondly, the FLC based EMS constructed with the new membership functions will control the generated new HESS to output the demand power from the battery and supercapacitor respectively. Then, the maximum number of laps can be obtained when both the battery and supercapacitor arrives at the minimum state of charge values set in the constraints, while the capacity loss of the battery is evaluated with the average current of the battery during the whole scenario. There are quite a lot of existing literature to model the capacity loss of the lithium-ion battery. The capacity loss model is mostly validated by discharging the battery with constant current C rate, and we haven't find any work that can predict the battery capacity loss dynamically with validated experimental work. Thus, we choose to estimate the capacity loss of the battery with average load as many previous work did. When the Pareto-frontier of the two evaluation indexes is obtained, the above iteration will terminate, otherwise, it will continue.

This work is dedicated to finding the optimal sizing parameter N_{sc} and the parameter vector x_{mf} defining the membership functions which are respectively the key parameters of the design and real-time FLC based EMS of the HESS. The optimized EMS will output the requested control command series $\mathbf{u}(t) = [P_{reqbat}, P_{reqsc}]$ to maximize the number of

traveled laps J_{laps} and battery cycle life $J_{lifebat}$ on a given race circuit:

$$\max J = [J_{laps}(\mathbf{x}(t), \mathbf{u}(t), \mathbf{p}), J_{lifebat}(\mathbf{x}(t), \mathbf{u}(t), \mathbf{p})] \quad (1)$$

subject to:

the first order dynamic constraints

$$\dot{\mathbf{x}}(t) = \mathbf{f}[\mathbf{x}(t), \mathbf{u}(t), t, \mathbf{p}], \quad (2)$$

the boundaries of the state, control and design variables

$$\begin{aligned} \mathbf{x}_{min} &\leq \mathbf{x}(t) \leq \mathbf{x}_{max} \\ \mathbf{u}_{min} &\leq \mathbf{u}(t) \leq \mathbf{u}_{max} \\ \mathbf{p}_{min} &\leq \mathbf{p} \leq \mathbf{p}_{max}, \end{aligned} \quad (3)$$

the algebraic path constraints

$$\mathbf{g}_{min} \leq \mathbf{g}[\mathbf{x}(t), \mathbf{u}(t), t, \mathbf{p}] \leq \mathbf{g}_{max}, \quad (4)$$

and the boundary conditions

$$\mathbf{b}_{min} \leq \mathbf{b}[\mathbf{x}(t_0), t_0, \mathbf{x}(t_f), t_f, \mathbf{p}] \leq \mathbf{b}_{max}, \quad (5)$$

where $\dot{\mathbf{x}}$ is the first order derivative of the state variables, \mathbf{f} is the dynamic model, \mathbf{x} , \mathbf{u} , \mathbf{p} are respectively the state, control and design vector with their lower and upper bounds: \mathbf{x}_{min} , \mathbf{u}_{min} , \mathbf{p}_{min} and \mathbf{x}_{max} , \mathbf{u}_{max} , \mathbf{p}_{max} . While \mathbf{g} and \mathbf{b} are the path and boundary equations respectively with their lower and upper bounds \mathbf{g}_{min} , \mathbf{b}_{min} and \mathbf{g}_{max} , \mathbf{b}_{max} .

In this work, the algebraic path constraint \mathbf{g} is eliminated by introducing a simple relaxation in Equation (12), the state variables \mathbf{x} , control variables \mathbf{u} , design parameters \mathbf{p} and the boundary constraints \mathbf{b} will be presented in the following paragraphs.

III. MODELLING OF THE HESS

The supercapacitor (SC) can output and absorb high peak power by controlling a bidirectional DC/DC converter that interfaces the supercapacitor to the DC link of the battery in parallel. Moreover, the voltage of supercapacitor can be used in a wide range with the help of the DC/DC converter [8]. There is a DC/AC inverter between the DC link and the AC motor that converts direct current to alternating current and power an employed AC motor. In particular, the DC/AC inverter allows a wide range input voltage from the DC link. In this section, the dynamic characteristics of the implemented Lithium-ion battery are analyzed first, and a dynamic battery model is employed after comparison. Then, the details of the employed battery cycle life model are presented. A simplified supercapacitor model is illustrated at the end of this section.

A. Dynamic Battery Model

The most existing battery models for the simulation of battery behavior basically include the experimental, electrochemical and electrical ones [24]. In order to obtain the optimal sizing parameters and energy management strategy for the HESS considering the characteristics of the battery in practical conditions, it is necessary to implement a proper dynamic battery model that can describe the battery dynamic behavior precisely. In this work, a modified Shepherd model is

employed to depict the dynamic characteristics of the battery during charging and discharging process [25]. The dynamic battery model are presented as Equation (6) and Equation (7) with the assumption that the internal resistance is constant and the thermal behavior of the battery is neglected.

Discharge:

$$V_{batt} = E_0 - K \frac{Q_{max}}{Q_{max} - it} it - K \frac{Q_{max}}{Q_{max} - it} i - Ri + Ae^{(-B \cdot it)} \quad (6)$$

Charge:

$$V_{batt} = E_0 - K \frac{Q_{max}}{Q_{max} - it} it - K \frac{Q_{max}}{it - 0.1Q_{max}} i - Ri + Ae^{(-B \cdot it)} \quad (7)$$

where V_{batt} is the battery voltage (V), E_0 is the voltage constant (V), K is the polarization constant or polarization resistance, Q_{max} is the total capacity, i is the battery current, R is the internal resistance. The battery discharge ($i > 0$) or charge ($i < 0$) it is denoted as

$$it = \int idt. \quad (8)$$

The calculation of the voltage amplitude A (V), time constant inverse B (Ah^{-1}) of the exponential zone, the polarization resistance K (Ω) and the voltage constant E_0 (V) in Equations (6) and (7) are referred to [25].

The state of charge of the battery x_{soc} and its derivative \dot{x}_{soc} is denoted as Equation (9) and Equation (10) respectively.

$$x_{soc} = 100 \left(1 - \frac{1}{3600Q_{max}} \int_0^{t_f} idt \right) \quad (9)$$

$$\dot{x}_{soc} = -\frac{1}{36Q_{max}} i \quad (10)$$

The charging/discharging i is denoted as

$$i = \begin{cases} \frac{P_{reqbat}}{N_{bat}V_{bat}\eta_{AD}}, & P_{reqbat} \geq 0 \\ \frac{P_{reqbat}\eta_{AD}}{N_{bat}V_{bat}}, & P_{reqbat} < 0 \end{cases} \quad (11)$$

where η_{AD} is the efficiency of the DC/AC converter taking into account of the motor efficiency as a constant value. In this work, the number of battery cells N_{bat} are determined by the available total mass of the HESS m_{HESS} and the number of the supercapacitor banks N_{sc} , as shown in Equation (12). The total mass of the HESS is fixed in this work considering the fact that the mass of a race car is strictly limited in general.

$$N_{bat} = \lfloor (m_{HESS} - N_{sc}m_{bank})/m_{cell} \rfloor \quad (12)$$

B. Battery Cycle Life Model

In recent years, substantial efforts have been made by both the researchers and industries to develop models that can predict the degradation of the lithium-ion batteries accurately [26]–[29]. A revised semi-empirical model based on Arrhenius equation is widely researched with large scale experiments, and this model is mostly applied in optimization and control problems related with batteries [26]. As presented from Equation (13) to Equation (16), the capacity loss of this model is

expressed as a function of the discharge current rate C_{rate} , temperature T and ampere-hour throughout A_h .

$$Q_{loss} = A \exp\left(\frac{-E_a}{RT}\right) (A_h)^z \quad (13)$$

where Q_{loss} represents the battery capacity loss, A the pre-exponential factor, E_a the activation energy from Arrhenius law (J), R is the gas constant of 8.314, T is the absolute temperature (K), A_h is the Ah-throughput, which represents the amount of charge delivered by the battery during cycling.

The pre-exponential factor A in Equation (13) is proved to be sensitive to the discharge current rate C_{rate} with large scale experiments in [30], and it is fitted with the format as Equation (14) in [31].

$$\ln A = a \cdot \exp(-b \cdot C_{rate}) + c \quad (14)$$

The activation energy can be fitted as a linear function of discharge current rate Ref. [30],

$$E_a = d + e \cdot C_{rate} \quad (15)$$

where a, b, c, d, e are the correction parameters of the battery cycle life model.

The Ah-throughput can be expressed as

$$A_h = \int_0^{t_f} \frac{i}{3600} dt \quad (16)$$

where i is the discharge current, t_f is the end time of the current profile.

C. Supercapacitor Model

In this work, the capacity fading of the supercapacitor is neglected considering the fact that it has much longer cycle life than lithium-ion batteries. The supercapacitor model is simplified to a series connection of a resistance and a supercapacitor bank [6]. Also, the efficiency of the DC/DC converter between the supercapacitor and the DC link is assumed to be a constant value of 0.95. The recursive supercapacitor model is deduced as

$$\dot{V}_{ct} = \begin{cases} -\frac{V_{ct} - \sqrt{V_{ct}^2 - 4R_{sct}P_{reqsc}/(\eta_{AD}\eta_{dc})}}{2C_{sct}R_{sct}} & P_{reqsc} \geq 0 \\ -\frac{V_{ct} - \sqrt{V_{ct}^2 - 4R_{sct}P_{reqsc}\eta_{AD}\eta_{dc}}}{2C_{sct}R_{sct}} & P_{reqsc} < 0 \end{cases} \quad (17)$$

$$x_{SOE} = \frac{V_{ct}^2}{V_{ctmax}^2} \quad (18)$$

where $V_{ct} = V_c N_{sc}$ is the total open circuit voltage of the supercapacitor pack assuming that all banks have a uniform behavior, t_{k+1} is the time at step $k+1$, R_{st} is the total equivalent series resistance, P_{reqsc} is the demand power from the supercapacitor, η_{dc} is the efficiency of the DC/DC converter, $C_{sct} = C_{bank}/N_{sc}$ is the total capacity, x_{SOE} is the state of energy, V_{ctmax} is the initial open circuit voltage, V_c is the open circuit voltage of one supercapacitor, N_{sc} is the total number of the banks, $R_s = N_{sc}R_s$ is the series resistance of one supercapacitor.

The actual total output power of the supercapacitor is represented as

$$P_{sc} = V_{ct} \cdot \frac{V_{ct} - \sqrt{V_{ct}^2 - 4R_{st}P_{reqsc}/\eta_{AD}\eta_{dc}}}{2R_{st}}. \quad (19)$$

IV. FLC BASED ON VECTORIZED FUZZY INFERENCE ENGINE

In this work, the EMS is developed based on fuzzy logic control (FLC), which has the features of real-time, adaptive and intelligent [32]–[34]. It allows different operators to merge nonlinearities and uncertainties in the best way and incorporate heuristic control in the form of if-then rules. The developed FLC in this section are composed of the if-then fuzzy rules, fuzzification, fuzzy inference engine and defuzzification modules. To speed up the optimization and take the advantage of the powerful matrix processing capability of MATLAB, a vectorized fuzzy inference system (VFIS) presented in Figure 2 is developed for the first time according to the state-of-the-art literature. The developed VFIS is capable to handle $N_p \times N_{inp}$ dimensional inputs with N_p pages of membership functions each time. This means that N_p fuzzy controllers (can be hundreds of thousands depends on the performance of the utilized CPU) can work at the same time with the same page number of inputs and outputs. The following paragraph will present the detail of fuzzy rules, membership functions, vectorized fuzzification, fuzzy inference engine, and defuzzification operations of the developed vectorized FLC.

A. Fuzzy Rules

Fuzzy rules are a set of if-then linguistic rules used to formulate the conditional relationships that comprise a fuzzy logic controller, for instance, a fuzzy rule can be: if SOE is *Small* and SOE is *Big* and P_{req} is *Positive big* then P_{sc} is *Positive big*. It is reasonable to devise the same if-then rules for the control of different sizes of HESSs since the control objectives of all the HESSs are the same in this work. The developed fuzzy rules are demonstrated as Figure 3 (a), where the labels N, P, S, M, B means negative, positive, small, medium and big respectively. The basic idea of the fuzzy rule is to utilize the supercapacitor as a buffer to reduce the high peak power impact on battery and absorb more regenerative braking power.

B. Membership Functions

The concept of membership functions was introduced by Zadeh in the first paper on fuzzy sets [35]. A membership function is a curve or a function that defines how each point of the input variables is mapped to a membership value between 0 and 1. It is quite challenging to design the optimal MFs for each HESS manually according to the engineering experiences. Besides, considering that the performance of the FLCs are sensitive to their MFs, different MFs of the FLCs with the same fuzzy rules should be devised for different sizes of HESS. Based on these considerations, the parameters of the MFs are selected as parts of the parameters to be optimized in this work.

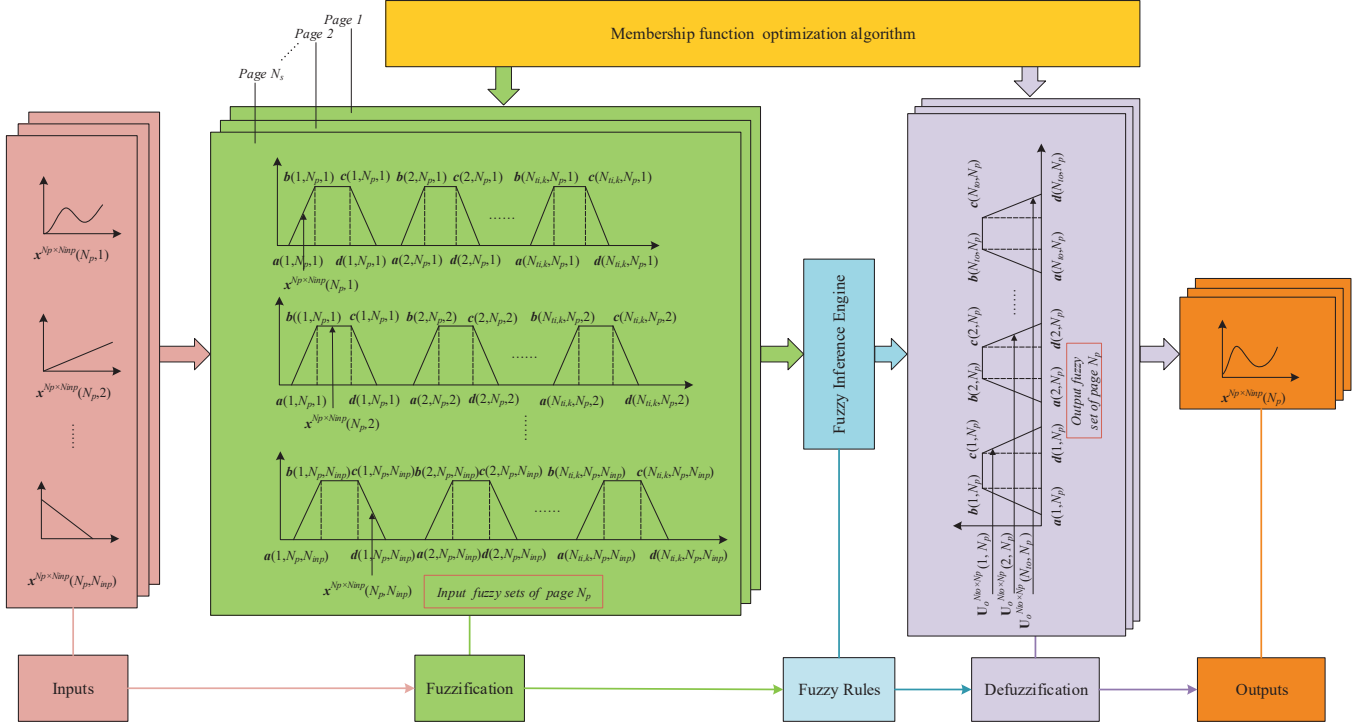


Fig. 2. Framework of the vectorized FLC

The trapezoidal-shaped membership function is selected for the fuzzy inference engine based on the considerations that it has high flexibility [11].

C. Vectorized Fuzzification

During the fuzzification stage, the input variables are identified to the fuzzy sets (membership functions) they belong to and the respective degree of membership to each relevance will be assigned. For a FIS with trapezoidal shaped MFs and a number of N_{inp} inputs, the fuzzy sets of each can be described with a matrix $\mathbf{S}_k = [\mathbf{a}_k, \mathbf{b}_k, \mathbf{c}_k, \mathbf{d}_k] \in \mathcal{R}^{N_p \times N_{ti,k} \times 4}$. N_p is the total page number of the inputs; $N_{ti,k}$ is the number of fuzzy linguistic sets of state input k , $k \in \{1, 2, \dots, N_{inp}\}$ and a, b, c, d are the variables that define one trapezoid in Figure ???. The input matrix is denoted as $\mathbf{x}_k \in \mathcal{R}^{N_p}$, for \mathbf{X}_k , its membership matrix $\boldsymbol{\mu}_k \in \mathcal{R}^{N_p \times N_{ti,k}}$ can be denoted as:

$$\begin{cases} \mu_k(\mathbf{a}_k \leq \mathbf{X}_k < \mathbf{b}_k) = \frac{\mathbf{X}_k - \mathbf{a}_k}{\mathbf{b}_k - \mathbf{a}_k} \\ \mu_k(\mathbf{b}_k \leq \mathbf{X}_k \leq \mathbf{c}_k) = \mathbf{I} \\ \mu_k(\mathbf{c}_k < \mathbf{X}_k \leq \mathbf{d}_k) = \frac{\mathbf{d}_k - \mathbf{X}_k}{\mathbf{d}_k - \mathbf{c}_k} \end{cases} \quad (20)$$

where $\mathbf{a}_k, \mathbf{b}_k, \mathbf{c}_k, \mathbf{d}_k, \mathbf{I}$ belong to $\mathcal{R}^{N_p \times N_{ti,k}}$, and \mathbf{X}_k is denoted as:

$$\mathbf{X}_k = \underbrace{[\mathbf{x}_k, \mathbf{x}_k, \dots, \mathbf{x}_k]}_{N_{ti,k}} \in \mathcal{R}^{N_p \times N_{ti,k}} \quad (21)$$

The membership array \mathbf{U} for input \mathbf{X} can be constructed as:

$$\mathbf{U} = \{\boldsymbol{\mu}_1, \dots, \boldsymbol{\mu}_k, \dots, \boldsymbol{\mu}_{N_{inp}}\} \in \mathcal{R}^{N_p \times N_{ti,k} \times N_{inp}} \quad (22)$$

D. Vectorized Fuzzy Inference Engine

Fuzzy inference is the way of mapping an input space to an output space using fuzzy logic. A FIS tries to formalize the reasoning process of human language by means of fuzzy logic (the built fuzzy If-Then rules). The process of fuzzy inference involves all of the MFs, If-Then rules, linguistic variables of the inputs and outputs. Mamdani's fuzzy inference method is the most commonly seen fuzzy methodology. The search-able fuzzy inference engine is able to map only one page of the inputs to one page of the outputs. This section will give an elaborate description of the developed powerful VFIS which allows a large number of FLCs operating in parallel based on Mamdani's fuzzy inference method.

The linguistic variables are programmed with their integer indexes from the smallest to the biggest in turn in this work. For instance, the fuzzy sets {NB, NM, NS, PS, PM, PB} of the third input in Figure 3 are correspondingly mapped to $\{1, 2, \dots, N_{ti,k}\}$, here $N_{ti,k} = 6$, $k = 3$. The fuzzy rule matrix $\mathfrak{R} \in \mathcal{R}^{N_r \times (N_{inp} + N_o)}$ is constructed with the mapped integer indexes, N_r is the number of fuzzy rules and N_o is the number of outputs. For instance:

$$\begin{array}{l} \text{Rule : } x_{SOC} \quad x_{SOE} \quad P_{req} \quad P_{sc} \\ \mathfrak{R}(N_r) : \quad 1 \quad 3 \quad 6 \quad 6 \end{array} \quad (23)$$

where $\mathfrak{R}(N_r)$ denotes the fuzzy rule N_r , it means the rule like: if SOC is *Small* and SOE is *Big* and P_{req} is *Positive big* then P_{sc} is *Positive big*. The working scheme of the VFIS is illustrated as follows:

1) Repeatedly copy the membership matrix $\boldsymbol{\mu}_k$ into N_r blocks,

and we can obtain:

$$\boldsymbol{\mu}_k^{temp} = \underbrace{[\boldsymbol{\mu}_k; \boldsymbol{\mu}_k; \dots; \boldsymbol{\mu}_k]}_{N_r}, \boldsymbol{\mu}_k^{temp} \in \mathcal{R}^{N_p \times N_{ti,k} \times N_r} \quad (24)$$

2) Create index matrix $\mathbf{L}_{in} \in \mathcal{R}^{N_p \times N_{ti,k} \times N_r}$ for input k :

$$\mathbf{L}_{in} = \left\{ \underbrace{\left[\begin{array}{cccc} 1 & 2 & \dots & N_{ti,k} \\ 1 & 2 & \dots & N_{ti,k} \\ \vdots & \vdots & \vdots & \vdots \\ 1 & 2 & \dots & N_{ti,k} \end{array} \right]}_{N_p}, \dots, \left[\begin{array}{cccc} 1 & 2 & \dots & N_{ti,k} \\ 1 & 2 & \dots & N_{ti,k} \\ \vdots & \vdots & \vdots & \vdots \\ 1 & 2 & \dots & N_{ti,k} \end{array} \right] \right\}_{N_r} \quad (25)$$

3) Repeatedly copy the k th column of the rule matrix $\mathfrak{R} \in \mathcal{R}^{N_r \times (N_{inp} + N_o)}$ into $N_p \times N_{ti,k}$ block arrangement $\mathfrak{R}_{temp} \in \mathcal{R}^{N_p \times N_{ti,k} \times N_r}$, $k \in \{1, 2, \dots, N_{inp}\}$:

$$\mathfrak{R}_{temp} = \left\{ \underbrace{\left[\begin{array}{cccc} \mathfrak{R}_k & \mathfrak{R}_k & \dots & \mathfrak{R}_k \\ \mathfrak{R}_k & \mathfrak{R}_k & \dots & \mathfrak{R}_k \\ \vdots & \vdots & \dots & \vdots \\ \mathfrak{R}_k & \mathfrak{R}_k & \dots & \mathfrak{R}_k \end{array} \right]}_{N_{ti,k}} \right\}_{N_p} \quad (26)$$

4) Get the effective membership matrix $\boldsymbol{\mu}_{eff,k}$ for input $k \in \{1, 2, \dots, N_{inp}\}$:

$$\boldsymbol{\mu}_{eff,k} = \boldsymbol{\mu}_k(L_{in} == \mathfrak{R}_{temp}), \boldsymbol{\mu}_{eff,k} \in \mathcal{R}^{N_p \times N_{ti,k} \times N_r} \quad (27)$$

5) Combine and get the final membership matrix $\mathbf{U}_{in} \in \mathcal{R}^{N_p \times N_r \times N_{inp}}$ for all the input \mathbf{X} :

$$\mathbf{U}_{in} = \underbrace{\left\{ \bigcup_{j=1}^{N_{ti,k}} \boldsymbol{\mu}_{eff,k}(j), \bigcup_{j=1}^{N_{ti,k}} \boldsymbol{\mu}_{eff,k}(j), \dots, \bigcup_{j=1}^{N_{ti,k}} \boldsymbol{\mu}_{eff,k}(j) \right\}}_{N_{inp}} \quad (28)$$

6) Get the mapped membership matrix \mathbf{U}_o for the output fuzzy sets:

$$\mathbf{U}_o = \bigcap_{k=1}^{N_{inp}} \mathbf{U}_{in}(k), \mathbf{U}_o \in \mathcal{R}^{N_p \times N_r} \quad (29)$$

7) Create index matrix $\mathbf{L}_o \in \mathcal{R}^{N_p \times N_r \times N_{to}}$ for output the fuzzy sets:

$$\mathbf{L}_o = \left\{ \underbrace{\left[\begin{array}{cccc} 1 & 2 & \dots & N_{to} \\ 1 & 2 & \dots & N_{to} \\ \vdots & \vdots & \vdots & \vdots \\ 1 & 2 & \dots & N_{to} \end{array} \right]}_{N_p}, \dots, \left[\begin{array}{cccc} 1 & 2 & \dots & N_{to} \\ 1 & 2 & \dots & N_{to} \\ \vdots & \vdots & \vdots & \vdots \\ 1 & 2 & \dots & N_{to} \end{array} \right] \right\}_{N_r} \quad (30)$$

8) Repeatedly copy the column of output fuzzy sets in the rule matrix $\mathfrak{R} \in \mathcal{R}^{N_r \times (N_{inp} + N_o)}$ into a $N_p \times N_{to}$ block arrangement $\mathfrak{R}_{otemp} \in \mathcal{R}^{N_p \times N_r \times N_{to}}$, N_{to} is the number of fuzzy linguistic sets of output :

$$\mathfrak{R}_{otemp} = \left\{ \underbrace{\left[\begin{array}{cccc} \mathfrak{R}_{N_o} & \mathfrak{R}_{N_o} & \dots & \mathfrak{R}_{N_o} \\ \mathfrak{R}_{N_o} & \mathfrak{R}_{N_o} & \dots & \mathfrak{R}_{N_o} \\ \vdots & \vdots & \dots & \vdots \\ \mathfrak{R}_{N_o} & \mathfrak{R}_{N_o} & \dots & \mathfrak{R}_{N_o} \end{array} \right]}_{N_{to}} \right\}_{N_p} \quad (31)$$

9) Repeatedly copy the membership matrix of the output fuzzy

sets $\mathbf{U}_o \in \mathcal{R}^{N_p \times N_r}$ into N_{to} blocks $\mathbf{U}_{o,temp}$:

$$\mathbf{U}_{o,temp} = \underbrace{\{\mathbf{U}_o, \mathbf{U}_o, \dots, \mathbf{U}_o\}}_{N_{to}}, \mathbf{U}_{o,temp} \in \mathcal{R}^{N_p \times N_r \times N_{to}} \quad (32)$$

10) Get the effective membership matrix $\mathbf{U}_{eff,o}$ of all the output fuzzy sets:

$$\mathbf{U}_{eff,o} = \mathbf{U}_{o,temp}(L_o == \mathfrak{R}_{otemp}), \mathbf{U}_{eff,o} \in \mathcal{R}^{N_p \times N_r \times N_{to}} \quad (33)$$

11) Merge the membership matrix of the output fuzzy sets in all the fuzzy rules

$$\mathbf{U}_{o,final} = \bigcup_{i=1}^{N_r} \mathbf{U}_{o,eff}(i), \mathbf{U}_{o,final} \in \mathcal{R}^{N_p \times N_{to}} \quad (34)$$

By the above calculation, the membership of each trapezoid of the output fuzzy set is obtained as $\mathbf{U}_{o,final}$, and the next step is the defuzzification.

E. Vectorized Defuzzification

The purpose of defuzzification process is to produce a quantifiable result in crisp logic based on the given fuzzy sets and corresponding membership degrees. The defuzzification process based on center of gravity method, the procedure of which is elaborated as followings:

1) Discrete the output fuzzy sets into N_{dis} parts $\mathbf{x}_o \in \mathcal{R}^{N_{dis}}$ from its minimum value $\mathbf{x}_{o,min}$ to the maximum one $\mathbf{x}_{o,max}$,

$$\mathbf{x}_o = [\mathbf{x}_{o,min} : (\mathbf{x}_{o,max} - \mathbf{x}_{o,min}) / (N_{dis} - 1) : \mathbf{x}_{o,max}] \quad (35)$$

where the value of N_{dis} affects the accuracy of the crisp output, for instance, the increasing of N_{dis} will improve the precision but will increase the computational burden.

2) Repeatedly copy $\mathbf{x}_o \in \mathcal{R}^{N_{dis}}$ and output fuzzy set $\mathbf{S}_o = [\mathbf{a}_o, \mathbf{b}_o, \mathbf{c}_o, \mathbf{d}_o] \in \mathcal{R}^{N_{to} \times N_p \times 4}$, we can obtain $\mathbf{x}_{o,temp} \in \mathcal{R}^{N_{to} \times N_p \times N_{dis}}$ and $\mathbf{S}_{o,temp} \in \mathcal{R}^{N_{to} \times N_p \times N_{dis}}$ respectively:

$$\mathbf{x}_{o,temp} = \underbrace{\left[\begin{array}{cccc} \mathbf{x}_o & \mathbf{x}_o & \dots & \mathbf{x}_o \\ \mathbf{x}_o & \mathbf{x}_o & \dots & \mathbf{x}_o \\ \vdots & \vdots & \dots & \vdots \\ \mathbf{x}_o & \mathbf{x}_o & \dots & \mathbf{x}_o \end{array} \right]}_{N_{to}} \right\}_{N_p} \quad (36)$$

$$\mathbf{S}_{o,temp} = \underbrace{[\mathbf{S}_o, \mathbf{S}_o, \dots, \mathbf{S}_o]}_{N_{dis}} \quad (37)$$

3) Calculate the membership matrix of $\mathbf{x}_{o,temp}$ based on the output fuzzy set $\mathbf{S}_{o,temp} = [\mathbf{a}_{o,temp}, \mathbf{b}_{o,temp}, \mathbf{c}_{o,temp}, \mathbf{d}_{o,temp}] \in \mathcal{R}^{N_{to} \times N_p \times N_{dis} \times 4}$:

$$\left\{ \begin{array}{l} \boldsymbol{\mu}_o(\mathbf{a}_{o,temp} \leq \mathbf{x}_{o,temp} < \mathbf{b}_{o,temp}) = \frac{\mathbf{x}_{o,temp} - \mathbf{a}_{o,temp}}{\mathbf{b}_{o,temp} - \mathbf{a}_{o,temp}} \\ \boldsymbol{\mu}_o(\mathbf{b}_{o,temp} \leq \mathbf{x}_{o,temp} \leq \mathbf{c}_{o,temp}) = \mathbf{I} \\ \boldsymbol{\mu}_o(\mathbf{c}_{o,temp} < \mathbf{x}_{o,temp} \leq \mathbf{d}_{o,temp}) = \frac{\mathbf{d}_{o,temp} - \mathbf{x}_{o,temp}}{\mathbf{d}_{o,temp} - \mathbf{c}_{o,temp}} \end{array} \right. \quad (38)$$

4) Repeatedly copy the membership matrix $\mathbf{U}_{o,final}$ in to N_{dis} blocks $\mathbf{U}_{o,temp} \in \mathcal{R}^{N_{to} \times N_p \times N_{dis}}$:

$$\mathbf{U}_{o,temp} = \underbrace{[\mathbf{U}_{o,final}, \mathbf{U}_{o,final}, \dots, \mathbf{U}_{o,final}]}_{N_{dis}} \quad (39)$$

5) Find the effective membership matrix:

$$\mathbf{U}_{eff,o} = \mathbf{U}_{o,temp} \cap \boldsymbol{\mu}_o, \mathbf{U}_{eff,o} \in \mathcal{R}^{N_{to} \times N_p \times N_{dis}} \quad (40)$$

6) Merge the membership matrix obtained in last step:

$$\mathbf{U}_{o,x} = \bigcup_{i=1}^{N_r} \mathbf{U}_{eff,o}(i), \mathbf{U}_{o,x} \in \mathcal{R}^{N_p \times N_{dis}} \quad (41)$$

7) Calculate the crisp output matrix for all the input matrices:

$$y = \frac{\sum_{i=1}^{N_{dis}} \mathbf{x}_o(i) \circ \mathbf{U}_{o,x}(\mathbf{x}_o(i))}{\sum_{i=1}^{N_{dis}} \mathbf{U}_{o,x}(\mathbf{x}_o(i))}, y \in \mathcal{R}^{N_p} \quad (42)$$

In order to design the fuzzy rules and membership functions conveniently, the devised vectorized FLC modules illustrated above are developed in MATLAB with standard and user friendly interfaces.

V. SIMULATION PARAMETERS AND SETTINGS

The state variables includes the battery state of charge x_{SOC} and state of energy of the supercapacitor x_{SOE} , $\mathbf{x} = [x_{SOC}, x_{SOE}]$. The control variable output by the FLC in this work is the requested power from the supercapacitor $\mathbf{u} = P_{reqsc}$, while the demand power from the battery can be calculated by $P_{reqbat} = P_{dem} - P_{reqsc}$. The design parameter vector is $\mathbf{p} = \{N_{sc}, \mathbf{x}_{mf}\}$. The designed fuzzy rules and initial membership functions are demonstrated in Figure 3, and there are 28 parameters of the devised membership functions plus one design parameter of the HESS in one page of parameters to be optimized. The design vector \mathbf{p} is constrained by defining \mathbf{p}_{min} and \mathbf{p}_{max} .

The operating profile of an electric race car is of great difference with the one of conventional electric vehicle running on a city road. Thus, standard driving cycles are not suitable for the research on electric race car. The real driving cycle of a race car in Nurburgring circuit is chosen as the test scenario. The demand driving/braking power is calculated by Equation (43). The corresponding velocity profile, acceleration profile and demand power are demonstrated as Figure 4.

$$P_{dem} = \left(\frac{1}{2} \rho C_d A v^2 + f m_v g + m_v a\right) v \quad (43)$$

The detail simulation parameters of the race car, 53 Ah (Rated) high energy lithium-ion battery, 2.85V/3400F high performance supercapacitor and the converters are illustrated in Table I.

In the FLC based EMS, the SOE and current of the supercapacitor are constrained between 0.1 and 0.99, -2000 A and 2000A respectively. While the SOC of the lithium-ion battery is constrained between 0.2 and 0.9, the current is regulated by adjusting the requested power from the battery. When the lithium-ion battery is exhausted, the simulation of

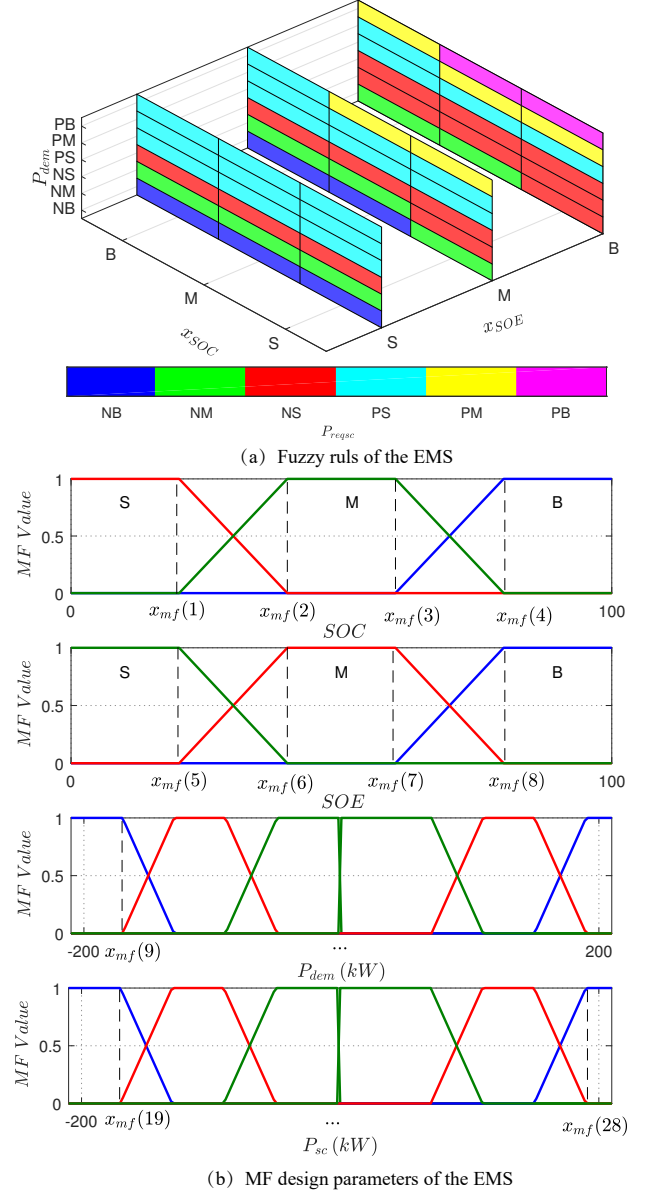


Fig. 3. Parameters of the FLC based EMS

one iteration will be terminated and the objective functions will be correspondingly evaluated. The temperature is for sure very important in any kind of vehicle equipped with batteries since it can affect the performance of the batteries directly. However, it is very difficult to model the heat generation, dissipation and the thermal control system of the energy storage system on an electric vehicle precisely. Actually, it is reasonable to assume that the temperature is controlled at a constant value (23 °C) by adjusting the thermal control system [1], [36].

In this work, a controlled elitist NSGA which is a variant of NSGA-II [37] is implemented to solve the multi-objective optimization problem. Instead of only choosing the top-ranking non-dominated fronts, the controlled elitist GA also favors individuals that can assist to improve the diversity of the population even if their fitness values are relatively lower.

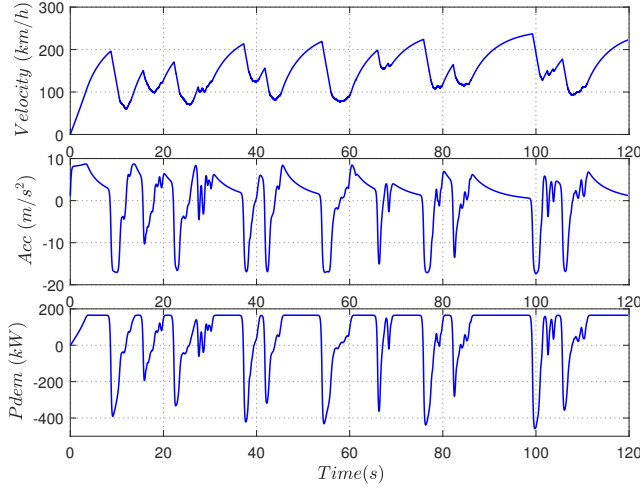


Fig. 4. Power demand in Nurburgring circuit

TABLE I
PARAMETER VALUES OF THE SIMULATION

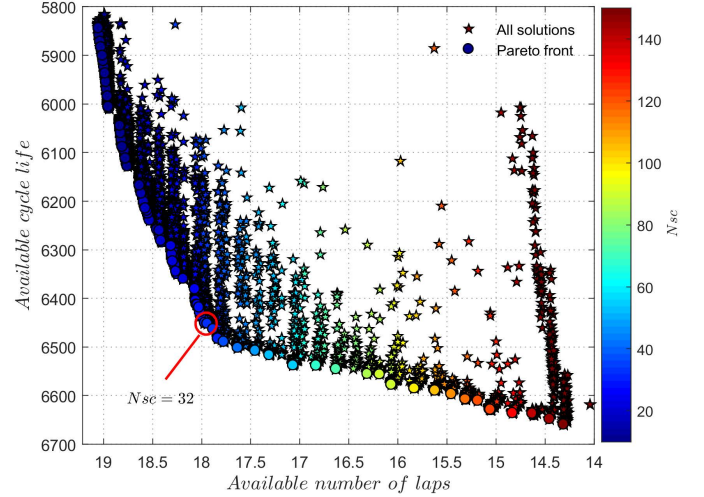
Parameters	Symbol	Value
Vehicle mass (kg)	m_v	570
Aerodynamics coefficient ($h^2 N/km^2$)	$\rho C_d A$	0.075
Rolling resistance coefficient	f	0.016
Mass of the battery cell (kg)	m_{cell}	1.15
Voltage constant of the battery cell (V)	E_0	3.43
Maximum capacity of the battery cell(Ah)	Q_{max}	55
Polarization resistance of the battery cell (Ω)	K	8.85×10^{-5}
Internal resistance of the battery cell (Ω)	R	1.33×10^{-3}
Voltage amplitude of the battery cell (V)	A	0.761
Time constant inverse of the battery cell (Ah^{-1})	B	0.040
Fitting parameter of pre-exponential factor	a	1.345
Fitting parameter of pre-exponential factor	b	0.2563
Fitting parameter of pre-exponential factor	c	9.179
Fitting parameter of activation energy	d	46868
Fitting parameter of activation energy	e	-470.3
Mass of the supercapacitor bank (kg)	m_{bank}	0.52
Supercapacitor bank capacity(F)	C_{bank}	3400
Supercapacitor equivalent series resistance (Ω)	R_s	2.2×10^{-4}
DC/DC converter efficiency	η_{dc}	0.95
DC/AC converter efficiency	η_{AD}	0.96

VI. RESULTS

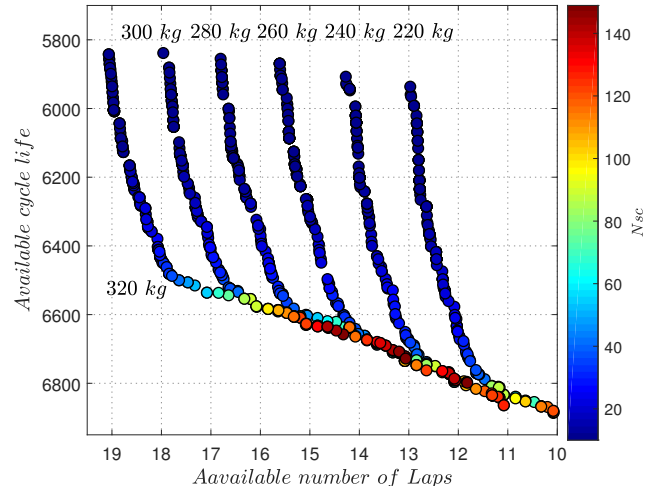
In this section, the results of the multi-objective optimal sizing and control of the HESS are presented and analyzed in detail. Figure 5 presented the achieved results when the total mass of the HESS is limited to 320 kg. The population size is set as 500 in the NSGA-II optimization algorithm, and the optimization is terminated after about 13 hours in a ThinkPad T470P laptop with Intel(R) Core(TM) i5-7300HQ CPU @2.50 GHz CPU and 16GB RAM, the number of total iterations is 1839.

From the sizing point of view, using different number of supercapacitors means different compromises between high power density and high energy density. As it is demonstrated in Figure 5, utilizing more supercapacitors can assist to reduce the average current of the Lithium-ion battery which is beneficial for longer cycle life of the battery, but cut down the energy density of the HESS which results in shorter driving mileage. When less supercapacitors are used, the results will

be opposite. It is also observed from Figure 5 that HESS with the same design solutions (makers filled with the same color) may achieve different values of both objective functions, which means that for the same HESS with uniform fuzzy rules, the parameters of the membership functions will determine whether we can achieve the Pareto optimal solutions. Thanks to the proposed Bi-level optimal sizing and control framework, the corresponding sizing parameter N_{sc} of each HESS and the membership function parameters \mathbf{x}_{mf} of the related EMS are coupled and obtained at the same time for all the solutions including those on the Pareto frontier.

Fig. 5. Multi-objective sizing and control solutions when $m_{HESS} = 320kg$

Moreover, this work has investigated the optimal sizing and control results of HESSs with different total mass. From Figure 6, we can draw the following basic conclusions: 1) HESSs with smaller total mass will cover fewer number of available laps, but the available cycle life of the battery are longer due to their shorter operating mileage; 2) We can achieve a pretty decent compromised solution that can enhance both objective functions with only about 40 supercapacitor banks and the optimized membership functions.

Fig. 6. Pareto optimal solutions for HESS with different mass m_{HESS}

In order to analyze the reason of the exhibited advantages of the proposed Bi-level optimal sizing and control framework, one solution from the Pareto frontier in Figure 5 ($N_{sc} = 32$) is compared with the solution with same sizing parameter but the initial devised membership functions. Figure 7 demonstrates the initial and optimized membership functions with the dotted lines and solid lines respectively.

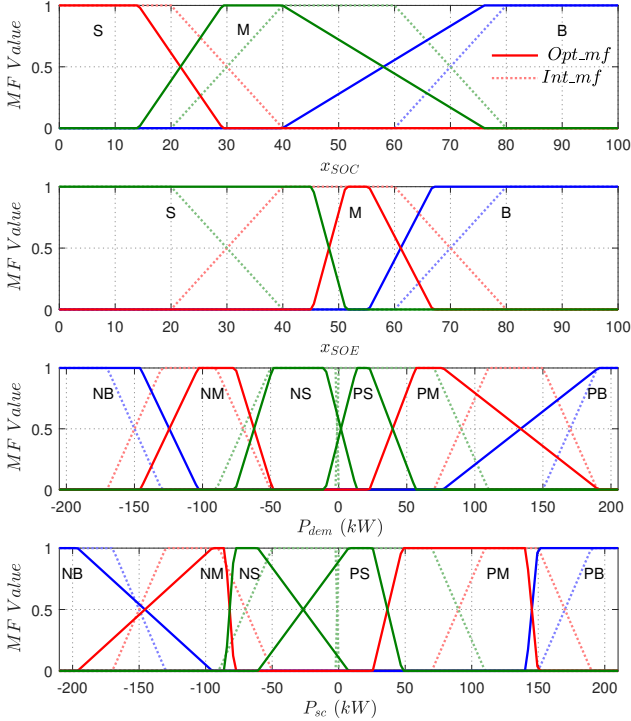


Fig. 7. The initial and optimized membership functions when $N_{sc} = 32$

The achieved available number of laps of the initial and optimized solutions are very similar which are respectively 17.88 and 17.98. This is mostly due to the fact that the two cases are implemented with the same HESS and the available mileage is mainly determined by the sizing parameters rather than the control parameters. However, the available cycle life of the battery are different which are respectively 6082 and 6463. This means that HESS with the optimized membership functions improved the battery cycle life by 6.3%. Figure 8 presents the interested variables between 0-200s, as it is illustrated in Figure 8 (a) and Figure 8 (b), the EMS with initial devised membership functions tends to request more high peak power from the battery and less from the supercapacitors which will accelerate the degradation of the battery. This phenomenon can be explained with the curve of *SOE* in Figure 8 (c). We can see that EMS with the initial devised membership functions tends to exhaust the supercapacitors very fast at a few seconds after starting the operation and the average *SOE* is under 20% during the simulation which is not capable to provide long-time high peak power to protect the battery. While EMS with the optimized membership functions tends to maintain the *SOE* of the supercapacitors above 50%, which helps to play the role of shaving the peak and filling the valley very well during the whole driving profile. For instance,

the curves in the dotted box in Figure 8 (c) demonstrate that the requested power from the battery is less after optimizing the MFs since the *SOE* is maintained at a relatively high level due to the optimized EMS.

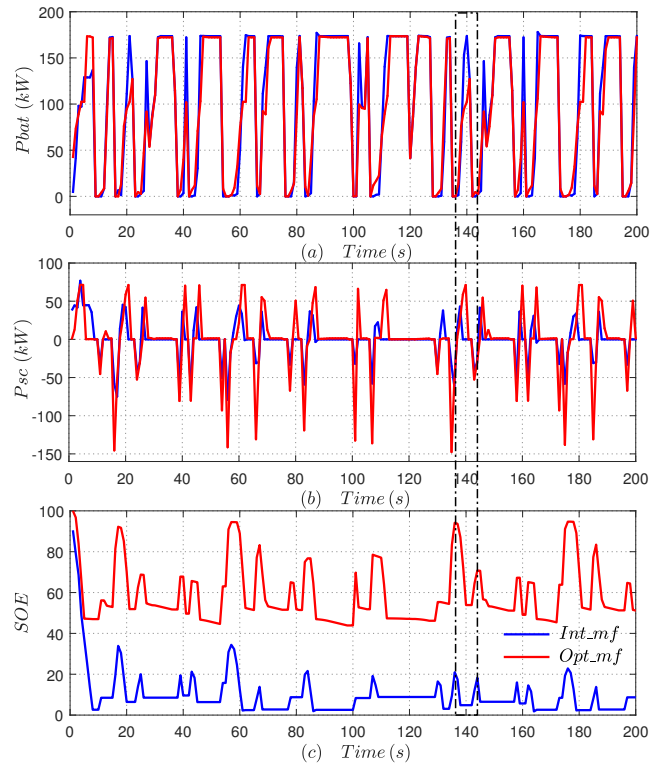


Fig. 8. Pareto optimal solutions for HESS with different MFs

VII. CONCLUSIONS

More supercapacitors do not always guarantee a better overall performance especially when the total mass of the HESS is limited due to the fact that the energy density of the supercapacitor is quite poor and it can be exhausted very fast even if it has high power density. However, we are able to obtain a pretty good balanced performance with less supercapacitors and the optimized EMS by the proposed optimization framework. The proposed Bi-level optimal sizing and control framework in this work makes it possible to obtain the global optimal solutions since it enables the optimization algorithm to search both the design and control parameters simultaneously. The user could choose the favored sizing solution from the obtained Pareto frontier packaged with the optimal membership functions based on a preferred compromise between the two objectives. The obtained global optimal sizing parameters and optimal parameters of the real-time controller on the Pareto frontier can be put into real-time implementations. In addition to the Bi-level optimal sizing and control framework, the devised vectorized fuzzy inference system with standard interfaces can be used in other kinds of real time feedback control problems, in particular, it can assist to dramatically improve the computational efficiency when needs to optimize the parameters of fuzzy logic controller.

REFERENCES AND FOOTNOTES

REFERENCES

- [1] X. Hu, L. Johannesson, N. Murgovski, and B. Egardt, "Longevity-conscious dimensioning and power management of the hybrid energy storage system in a fuel cell hybrid electric bus," *Applied Energy*, vol. 137, pp. 913–924, 2015.
- [2] G. Suri and S. Onori, "A control-oriented cycle-life model for hybrid electric vehicle lithium-ion batteries," *Energy*, vol. 96, pp. 644–653, 2016.
- [3] F. Sun, X. Hu, Y. Zou, and S. Li, "Adaptive unscented Kalman filtering for state of charge estimation of a lithium-ion battery for electric vehicles," *Energy*, vol. 36, no. 5, pp. 3531–3540, 2011.
- [4] Y. Zou, X. Hu, H. Ma, and S. E. Li, "Combined state of charge and state of health estimation over lithium-ion battery cell cycle lifespan for electric vehicles," *Journal of Power Sources*, vol. 273, no. Supplement C, pp. 793 – 803, 2015.
- [5] A. Burke, "Ultracapacitors: why, how, and where is the technology," *Journal of power sources*, vol. 91, no. 1, pp. 37–50, 2000.
- [6] L. Zhang, X. Hu, Z. Wang, F. Sun, and D. G. Dorrell, "A review of supercapacitor modeling, estimation, and applications: A control/management perspective," *Renewable and Sustainable Energy Reviews*, vol. 81, pp. 1868 – 1878, 2018.
- [7] S. M. Lukic, S. G. Wirasingha, F. Rodriguez, J. Cao, and A. Emadi, "Power management of an ultracapacitor/battery hybrid energy storage system in an hev," in *2006 IEEE Vehicle Power and Propulsion Conference*, Sept 2006, pp. 1–6.
- [8] J. Cao and A. Emadi, "A new battery/ultracapacitor hybrid energy storage system for electric, hybrid, and plug-in hybrid electric vehicles," *IEEE Transactions on power electronics*, vol. 27, no. 1, pp. 122–132, 2012.
- [9] T. Ma, H. Yang, and L. Lu, "Development of hybrid battery-supercapacitor energy storage for remote area renewable energy systems," *Applied Energy*, vol. 153, pp. 56–62, 2015.
- [10] C. G. Hochgraf, J. K. Basco, T. P. Bohn, and I. Bloom, "Effect of ultracapacitor-modified PHEV protocol on performance degradation in lithium-ion cells," *Journal of Power Sources*, vol. 246, pp. 965–969, 2014.
- [11] H. Yu, D. Tarsitano, X. Hu, and F. Cheli, "Real time energy management strategy for a fast charging electric urban bus powered by hybrid energy storage system," *Energy*, vol. 112, pp. 322–331, 2016.
- [12] J. Shen, S. Dusmez, and A. Khaligh, "Optimization of sizing and battery cycle life in battery/ultracapacitor hybrid energy storage systems for electric vehicle applications," *IEEE Transactions on Industrial Informatics*, vol. 10, no. 4, pp. 2112–2121, 2014.
- [13] Z. Song, J. Li, X. Han, L. Xu, L. Lu, M. Ouyang, and H. Hofmann, "Multi-objective optimization of a semi-active battery/supercapacitor energy storage system for electric vehicles," *Applied Energy*, vol. 135, no. 0, pp. 212–224, 2014.
- [14] X. Hu, N. Murgovski, L. M. Johannesson, and B. Egardt, "Comparison of three electrochemical energy buffers applied to a hybrid bus powertrain with simultaneous optimal sizing and energy management," *IEEE Transactions on Intelligent Transportation Systems*, vol. 15, no. 3, pp. 1193–1205, 2014.
- [15] S. F. Tie and C. W. Tan, "A review of energy sources and energy management system in electric vehicles," *Renewable and Sustainable Energy Reviews*, vol. 20, pp. 82 – 102, 2013.
- [16] H. Yin, C. Zhao, M. Li, and C. Ma, "Utility Function-Based Real-Time Control of A Battery Ultracapacitor Hybrid Energy System," *IEEE Transactions on Industrial Informatics*, vol. 11, no. 1, pp. 220–231, 2015.
- [17] S. Dusmez and A. Khaligh, "A supervisory power splitting approach for a new ultracapacitor battery vehicle deploying two propulsion machines," *IEEE Transactions on Industrial Informatics*, vol. 10, no. 3, pp. 1960–1971, 2014.
- [18] B. Hredzak, V. G. Agelidis, and G. Demetriades, "Application of explicit model predictive control to a hybrid battery-ultracapacitor power source," *Journal of Power Sources*, vol. 277, pp. 84–94, 2015.
- [19] Q. Zhang, W. Deng, and G. Li, "Stochastic Control of Predictive Power Management for Battery/Supercapacitor Hybrid Energy Storage Systems of Electric Vehicles," *IEEE Transactions on Industrial Informatics*, pp. 1–1, 2017.
- [20] K. Jia, Y. Chen, T. Bi, Y. Lin, D. Thomas, and M. Sumner, "Historical-Data-Based Energy Management in a Microgrid With a Hybrid Energy Storage System," *IEEE Transactions on Industrial Informatics*, vol. 13, no. 5, pp. 2597–2605, 2017.
- [21] J. Shen and A. Khaligh, "Design and real-time controller implementation for a battery-ultracapacitor hybrid energy storage system," *IEEE Transactions on Industrial Informatics*, vol. 12, no. 5, pp. 1910–1918, 2016.
- [22] H. Yu, F. Castelli-Dezza, and F. Cheli, "Optimal powertrain design and control of a 2-ibd electric race car," in *2017 International Conference of Electrical and Electronic Technologies for Automotive*, June 2017, pp. 1–7.
- [23] X. Hu, S. J. Moura, N. Murgovski, B. Egardt, and D. Cao, "Integrated Optimization of Battery Sizing, Charging, and Power Management in Plug-In Hybrid Electric Vehicles," *IEEE Transactions on Control Systems Technology*, vol. 24, no. 3, pp. 1036–1043, may 2016.
- [24] T. Liu, X. Hu, S. E. Li, and D. Cao, "Reinforcement Learning Optimized Look-Ahead Energy Management of a Parallel Hybrid Electric Vehicle," *IEEE/ASME Transactions on Mechatronics*, vol. 22, no. 4, pp. 1497–1507, aug 2017.
- [25] O. Tremblay, L.-a. Dessaint, and a. I. Dekkiche, "A Generic Battery Model for the Dynamic Simulation of Hybrid Electric Vehicles," *2007 IEEE Vehicle Power and Propulsion Conference*, no. V, pp. 284–289, 2007.
- [26] J. Wang, P. Liu, J. Hicks-Garner, E. Sherman, S. Soukiazian, M. Verbrugge, H. Tataria, J. Musser, and P. Finamore, "Cycle-life model for graphite-LiFePO4 cells," *Journal of Power Sources*, vol. 196, no. 8, pp. 3942–3948, 2011.
- [27] C. Zhang, Y. Zhang, and Y. Li, "A Novel Battery State-of-Health Estimation Method for Hybrid Electric Vehicles," *IEEE/ASME Transactions on Mechatronics*, vol. 20, no. 5, pp. 2604–2612, oct 2015.
- [28] X. Hu, D. Cao, and B. Egardt, "Condition Monitoring in Advanced Battery Management Systems: Moving Horizon Estimation Using a Reduced Electrochemical Model," *IEEE/ASME Transactions on Mechatronics*, vol. 23, no. 1, pp. 167–178, feb 2018.
- [29] C. Zou, C. Manzie, and D. Nestic, "Model Predictive Control for Lithium-Ion Battery Optimal Charging," *IEEE/ASME Transactions on Mechatronics*, vol. X, no. X, pp. 1–10, 2018.
- [30] R. Wang, Y. Chen, D. Feng, X. Huang, and J. Wang, "Development and performance characterization of an electric ground vehicle with independently actuated in-wheel motors," *Journal of Power Sources*, vol. 196, no. 8, pp. 3962–3971, 2011.
- [31] J. Shen, A. Hasanzadeh, and A. Khaligh, "Optimal power split and sizing of hybrid energy storage system for electric vehicles," in *2014 IEEE Transportation Electrification Conference and Expo (ITEC)*, 2014, pp. 1–6.
- [32] J. A. Cabrera, J. J. Castillo, E. Carabias, and A. Ortiz, "Evolutionary Optimization of a Motorcycle Traction Control System Based on Fuzzy Logic," *IEEE Transactions on Fuzzy Systems*, vol. 23, no. 5, pp. 1594–1607, oct 2015. [Online]. Available: <http://ieeexplore.ieee.org/document/6955819/>
- [33] F. Sabahi and M. R. Akbarzadeh-T, "Extended Fuzzy Logic: Sets and Systems," *IEEE Transactions on Fuzzy Systems*, vol. 24, no. 3, pp. 530–543, jun 2016. [Online]. Available: <http://ieeexplore.ieee.org/document/7152883/>
- [34] T. Wang, Y. Zhang, J. Qiu, and H. Gao, "Adaptive Fuzzy Backstepping Control for A Class of Nonlinear Systems With Sampled and Delayed Measurements," *IEEE Transactions on Fuzzy Systems*, vol. 23, no. 2, pp. 302–312, apr 2015. [Online]. Available: <http://ieeexplore.ieee.org/document/6767091/>
- [35] L. Zadeh, "Fuzzy sets," *Information and Control*, vol. 8, no. 3, pp. 338 – 353, 1965.
- [36] S. Ebbesen, P. Elbert, and L. Guzzella, "Battery state-of-health perceptive energy management for hybrid electric vehicles," *IEEE Transactions on Vehicular Technology*, vol. 61, no. 7, pp. 2893–2900, Sept 2012.
- [37] K. Deb, "Multi-objective optimization using evolutionary algorithms: an introduction," *Multi-objective evolutionary optimisation for product design and manufacturing*, pp. 1–24, 2011.